Available online at www.sciencedirect.com

ScienceDirect

Procedia CIRP 13 (2014) 365 – 370

www.elsevier.com/locate/procedia

2nd CIRP 2nd CIRP Conference on Surface Integrity (CSI)

Empirical modeling of residual stress profile in machining nickel-based superalloys using the sinusoidal decay function

D. Ulutan[a]*, Y.M. Arisoy[b], T. Özel[b], L. Mears[a]

[a]*Clemson University, International Center for Automotive Research, 4 Research Drive, Greenville, SC 29607, USA*
[b]*Rutgers University, Manufacturing & Automation Research Laboratory, Industrial & Systems Engineering, Piscataway, NJ 08854, USA*
* Corresponding author. Tel.: +1-401-932-7096; fax: +1-864-283-7225. *E-mail address*: dulutan@clemson.edu.

Abstract

After machining nickel-based superalloys, tensile surface residual stresses can cause end-product issues such as fatigue failure. Modeling the residual stress profile is currently tedious and inaccurate. This study introduces a new method of understanding the residual stress profile in terms of quantifiable key measures: peak tensile stress at the surface, magnitude and depth of peak compressive stress, and depth at which residual stress becomes near-zero. Experiments in turning IN-100 and milling GTD-111 have been conducted and subsequent X-ray Diffraction measurements have been utilized to obtain residual stress profiles. Using a sinusoidal decay function fitted to measured residual stress profiles, these four key profile measures are extracted and then the effects of process parameters such as cutting speed, feed, cutting edge radius, and tool coating on these measures are investigated.

Selection and peer-review under responsibility of The International Scientific Committee of the "2nd Conference on Surface Integrity" in the person of the Conference Chair Prof Dragos Axinte dragos.axinte@nottingham.ac.uk

Keywords: Machining; Nickel alloy; Residual stress

1. Introduction

Superalloys have recently found significant use in applications in the aerospace, automotive, energy, and biomedical industries [1]. Nickel-based superalloys are an important portion of these superalloys. Their superior properties improve even further with increasing material development. These properties are their high strength, as well as corrosion and creep resistance at elevated temperatures [2]. However, these properties make them very difficult to machine, because while machining these superalloys, high machining forces are observed and the cutting tool wears rapidly, decreasing productivity [3]. In addition, rapid work hardening behavior and poor thermal diffusivity cause reduced machining efficiency by enforcing the use of milder cutting conditions [4]. Consequently, when compromise from productivity and efficiency are not possible, the quality of the machined surface can deteriorate. Surface quality measures such as surface roughness and depth of machining affected zone can be used to improve their machinability, and many researchers have studied optimization of machining superalloys by analyzing these outputs [5-8]. However, the residual stress profile gives a more comprehensive understanding of the likelihood of fatigue failure due to crack initiation and propagation [9].

Fatigue failure is started with a crack initiated on the surface, which then propagates into the bulk of the material [10]. The affected section of the material is capable of withstanding a lower load, and when that load is exceeded, fatigue failure occurs. Thus, it is essential to understand and prevent the initiation of the crack.

During machining processes, thermo-mechanical loads cause elasto-plastic stresses on the workpiece material [11]. Due to these plastic stresses, surface of the material exhibits "residual" stresses even after removal of the loads, which causes the fatigue failure of the product [10]. Hence, it is important to reduce residual stresses as much as possible, and result in favorable (compressive) residual stresses.

For this purpose, many researchers worked on experimentally measuring residual stresses using different methods [6-17]. While hole drilling and other

Selection and peer-review under responsibility of The International Scientific Committee of the "2nd Conference on Surface Integrity" in the person of the Conference Chair Prof Dragos Axinte dragos.axinte@nottingham.ac.uk
doi:10.1016/j.procir.2014.04.062

destructive methods are also used in some applications, for processes (such as machining) where the residual stresses diminish rapidly below the surface, more precise methods such as X-ray diffraction (XRD) are used. In these studies, researchers aim to understand and analyze residual stress profiles, and the effects of different machining parameters. However, due to the high uncertainty of results in residual stress measurements and the big difference in the behaviors of different materials, these profiles can exhibit different characteristics that lead to a lack of consensus. In addition, measuring residual stresses using XRD is very costly and it becomes impractical and expensive to test for different conditions, and replicate tests to reduce variation. Therefore, while the experimental studies are very important in providing the baseline data, residual stress research cannot only rely on experimentation.

There have been many modeling efforts regarding surface residual stresses as well as residual stress profiles. Analytically modeling residual stress is one way, where different assumptions (such as plain strain or plain stress conditions) are employed in calculating the residual stresses using physical equations. However, these models represent the ideal conditions of events and usually are not practically applicable [11,13,18-20].

Researchers have tried to analyze and predict residual stresses using Finite Element-based models [21-24]. These efforts usually provide a good understanding of the process and its results. However, they involve many assumptions; and even when experimentally validated, they can lack the capability of predicting other tests. Also, when their capabilities are improved by decreasing the element size or time step, the computation cost can be too high to account for their value.

Finally, some researchers have modeled the residual stress profile using statistically fitted polynomial functions [9,25]. Yet the profile does not necessarily resemble a polynomial fit, particularly when only few terms are used. When many terms are used, the model becomes complex and not easily applicable to other processes, materials, or machining conditions. However, the profile can be better represented with a function that it resembles such as a sinusoidal decay function, which also has a fixed number of terms. Therefore, without increasing the complexity of the mathematical model, it is possible to represent any residual stress profile.

This work aims to fill the void in empirically modeling residual stress profile using such a sinusoidal decay function, and obtaining the four key measures of a residual stress profile. These measures are identified as the peak residual stress at the surface (*PTS*), magnitude (*PCS*) and location (*PCD*) of the peak compressive residual stress, and the settling distance (*SD*), which is the distance where the residual stresses become near-zero. Then, these measures can be easily optimized as required by modifying the machining parameters. *PTS* has been shown to be the main cause for crack initiation in fatigue failure, *PCS* and *PCD* are mainly related to dimensional accuracy of the end product, and *SD* indicates where the effects of the process diminish: the end of the machining affected zone.

In order to accomplish this task, first milling and turning experiments are conducted on nickel-based superalloys GTD-111 and IN-100. Residual stresses are measured using XRD technique at different depth levels on the machined surface. A sinusoidal decay function is fit to these measurements, and the coefficients of this function are found for each profile. Particle Swarm Optimization (*PSO*) method is used to minimize the difference (error) between the measurements and the mathematical model, and therefore obtain the coefficients that fit the model. The four identified key measures (*PTS*, *PCS*, *PCD*, *SD*) are calculated, and then the effects of machining parameters on these key measures are determined.

$a_{1\text{-}2}$	acceleration constants
f	feed per revolution
$\mathbf{g}$	global best position vector
i & n	particle and iteration numbers
$\mathbf{p_i}$	best position vector of particle i
x	depth below the surface
$\mathbf{x_i^n}$	position vector of particle i at iteration n
v_c	cutting speed
$\mathbf{v_i^n}$	velocity vector of particle i at iteration n
C	coefficient of the sinusoidal decay function
N & N'	total number of iterations & number of trials
PCD	depth of peak compressive residual stress
PCS	magnitude of peak compressive residual stress
PTS	magnitude of residual stress at the surface
SD	settling distance of residual stress profile
δ'	random disturbance
ζ	damping coefficient
ω_0-ω_d	undamped and damped frequencies
ϕ	phase angle

2. Experiments

2.1. Milling GTD-111

Milling experiments on GTD-111 were conducted in the Clemson University – International Center for Automotive Research (CU-ICAR). A rectangular block of GTD-111 with dimensions of 120 x 70 x 30 mm^3 was prepared, and an indexable Sandvik tool (15.875 mm diameter) was used, with two multi-layer TiAlN coated tungsten carbide inserts of type "R390-11T308M-PM 1030". Coolant was flooded on the tool-workpiece contact zone throughout the duration of the test. Two factors (cutting speed and feed) were tested for this

material. Three levels of cutting speed (25, 50, and 100 m/min) and two levels of feed (0.05 and 0.2 mm/rev) were employed. The rectangular block was set up in an OKUMA GENOS M460-VE 3-axis CNC vertical milling machine, and all other parameters were kept constant throughout the experiments for consistency, with a 9.5 mm width of cut (manufacturer limit of 60% tool engagement) and 0.5 mm depth of cut.

2.2. Turning IN-100

Face turning experiments on the nickel-based superalloy IN-100 (typically obtained via powder metallurgy route and used as disc superalloy for aircraft engines) were conducted in the Manufacturing & Automation Research Laboratory of Rutgers University to see the effects of cutting edge radius and addition of coating. A 113 mm diameter IN-100 disc was prepared, and a TPG432 insert type tool with a 0.8 mm nose radius and a 11° relief angle was used. Uncoated WC/Co tools with three different edge radii (Sharp, 10, and 25 μm) were used, and a layer of TiAlN coating was applied on a sharp tool to have a tool with approximately 10 μm edge radius. Cutting speed, feed, and depth of cut were fixed at 24 m/min, 0.05 mm/rev, and 1 mm respectively.

2.3. Residual stress measurements

Machining-induced residual stresses were measured using XRD on the rectangular blocks of GTD-111 and thin discs of IN-100 at 6 different depths: at the surface, and approximately 10, 25, 50, 80, and 125 μm deep below the surface. For the end-milled GTD-111 blocks, longitudinal residual stresses were measured, and for the face turned IN-100 disks, circumferential and radial residual stresses were measured [24,29]. Depth levels were selected in such a fashion that most (if not all) of the features of the residual stress profile could be captured. A ProtoXRD unit with Mn-Cu-K_α radiation (2.1Å wavelength) at 17 kV and 4 mA, and 1x2 mm beam spot size was used to acquire diffraction peaks at 155° 2θ angles for the {311} Miller indices. Surface was electropolished after each layer of measurement to obtain results from each successive layer of machined workpiece, and therefore obtain residual stress profiles of each test along the depth of the material. Results showed that the standard error is low (5-10% of the value of the peak compressive stress).

3. Modeling

3.1. Sinusoidal decay function

Although researchers have created mathematical models to fit functions to the residual stress profiles, these models have been limited to polynomial fits [9,25]. With polynomial fits, the advantage is the freedom in determination of the number of terms (thus the number of coefficients). The order of the polynomial can be set to any value up to one less than the number of data points, requiring a degree of subjectivity by the modeler.

However, it is determined by researchers that the residual stress profile after machining conventionally follows a similar pattern: A tensile (or small compressive) peak at the surface, followed by a compressive peak, settling at a distance without becoming positive again, or very small positive values [1-3]. On one hand, it is possible to represent this behavior using polynomial fits, but many terms may be needed to model with good accuracy. On the other hand, it is possible to represent this behavior using a sinusoidal decay function, as it resembles the underdamped oscillation of an impulse-loaded spring-mass-damper system. Such a system can be represented using Eq. (1). With such a function, the number of terms in the equation is fixed, and the model never becomes more complex. Since the residual stress profile resembles the sinusoidal decay curve (and the fact that a third order polynomial may not be able to represent such behavior), this model could be applied to residual stress profiles of different materials, processes, or machining conditions. Only when a residual stress profile that does not follow a sinusoidal decay behavior is observed, this model will not be able to represent the data. This is usually the case with destructive methods of residual stress measurement such as hole drilling, which is not suitable for immediate sub-surface residual stress measurements.

$$\sigma = Ce^{-\varsigma\omega_0 x}\cos(\omega_d x + \phi) \quad (1)$$

The surface stress is represented with both amplitude and phase angle, so there is no need to have any restrictions on either. Therefore, phase angle is ranged between ϕ=[–π, +π], and the amplitude is ranged between C=[0, 10000] MPa. Negative values are not included because phase angle covers the whole range of stress, and narrowing the search domain increases the search quality. The damped frequency is proportional to the inverse of the period of the wave, and since it was estimated that the function would settle around 200 μm, ω_d is restricted to [0, 0.06] mm^{-1}. At lower ω_d, the period of the wave gets longer, representing deeper settling distances. At ω_d values close to 0.06 mm^{-1}, period of the wave (distance between two compressive peaks) can get as small as 100μm. The undamped frequency is related to the damped frequency and the damping coefficient through Eq. (2), so it is not searched separately.

$$\omega_0 = \frac{\omega_d}{\sqrt{1-\varsigma^2}} \quad (2)$$

The damping coefficient (ς) is important in defining how quickly the wave will settle to a near-zero value.

Since the desired shape is underdamped, this coefficient is mathematically upper-limited at 1. On the other hand, if a wave is only slightly damped (e.g. ς<0.5), it would oscillate between positive and negative many times, and the residual stress profiles conventionally do not exhibit such behavior. Therefore, the damping coefficient is also lower-limited at 0.7. Although these limitations may be counter-productive against having a full-scale search, they allow higher resolution in the domain for the same computational cost. At the end of each search, if any parameter is found to be at its limits, the constraints are loosened to search for better solutions. However, it is observed that this loosening of the constraints did not provide any improvement in minimizing the error.

3.2. Particle swarm optimization

In order to find the coefficients of the best sinusoidal decay function that fits the experiments, the difference between the model and the measurements (to be minimized) is found in all experimental points. For polynomial fits, particularly for lower order functions, calculation of the objective function is straightforward. However, for a sinusoidal decay function, an easy direct computation of the coefficients is not available. Therefore, some type of a search algorithm is needed.

For this reason, Particle Swarm Optimization (PSO) is selected to obtain such coefficients that minimize the objective function. PSO is an evolutionary method similar to genetic algorithms, which is widely used for machining process optimization [26-29]. In this method, a set of particles is initialized at random combinations of decision variables; in this case, the four identified coefficients of Eq. (1). Then, the objective function is calculated for each particle, and the best solution is identified. Then, each particle is assigned a velocity (Eq. 3), which determines their position in the next iteration (Eq. 4). The factors affecting the velocity vector of a particle ($\mathbf{v_i^{n+1}}$) in Eq. (3) are the two predetermined acceleration constants (a_1 and a_2), best position vector of the particle ($\mathbf{p_i}$), best position vector of any particle ($\mathbf{g}$), position vector of the particle at the current iteration ($\mathbf{x_i^n}$), and a random disturbance (δ') in [-1,1] to ensure the particle is not stuck at local minima and possible improvements are not missed. The position of particle i is determined by adding its updated velocity multiplied by a factor K to its current position (Eq. 4). At the initial iterations, K is big so that particles move around more freely and investigate the whole domain. As the iterations progress, K is lowered (inversely proportional to n), allowing the particles to "fine tune" their position. The particle and global best vectors pull the particles toward them to ensure they investigate the right regions.

$$\mathbf{v}_i^{n+1} = \mathbf{v}_i^n + a_1(\mathbf{p}_i - \mathbf{x}_i^n) + a_2(\mathbf{g} - \mathbf{x}_i^n) + \delta \qquad (3)$$

$$\mathbf{x_i^{n+1}} = \mathbf{x_i^n} + K\mathbf{v_i^{n+1}} \qquad (4)$$

At each iteration and for every particle, the bounds are checked. So, if the velocity of a particle exceeds a predetermined value, it is set to be that limiting value. The limitation on the velocity ensures that the particles do not make any erratic movements. Also, if the position of a particle gets out of bounds, then it is set to the bounding value. This way, all particles are maintained within the domain. After checking the bounds, the objective function is calculated, and personal and global best positions are updated. Iterations go on until a predetermined number of iterations (N) are finished, and it was determined that N=50 iterations are satisfactory for this algorithm to settle to a value. A total of 10000 particles are used to ensure that every region within the field is covered. Also, the whole search is repeated N'=30 times so that an average value for the best solutions can be reached. This averaging ensures that if there is a search that results in an unexpected result, that search is isolated and the remaining results indicate such a behavior. In the end, if the best of the N'=30 results is not within one standard deviation of the average of the 30 results, the whole algorithm is repeated. However, it is important to note that such a repetition was never needed for the results presented in this work.

4. Results

Applying the mathematical model to the machining experiments, Eq. (1) coefficients and four key identifiers of the residual stress profile (*PTS*, *PCS*, *PCD*, *SD*) are calculated. In addition, R^2 values were calculated (Eq. 5) to display the goodness of the fit. In this equation, σ_{fit} is the residual stress fitted by the model at a measurement point, σ_{exp} is the experimental findings, and $\bar{\sigma}$ is the average of the experiments. The higher the R^2 value, the better the model fits the experimental results.

$$R^2 = 1 - \frac{\Sigma(\sigma_{fit} - \sigma_{exp})^2}{\Sigma(\sigma_{exp} - \bar{\sigma})^2} \qquad (5)$$

Table 1 shows the results of the model for end-milled GTD-111. The first six lines are the experimental findings used to develop the model, whereas the last line is used for confirming the results. It was observed that the R^2 values changed between 67 to 93%, meaning that the model fits the experimental findings well for most of the data points. Figure 1 shows the worst and the best fits for this material. It was observed from both the experiments and the model that the residual stress at the surface was compressive for all the cases, which is why the phase angle ϕ was above 90° for all cases. The damping coefficient was either very close to 1 indicating very small oscillation (if any), or very close to the lower

limit (0.7) indicating more oscillations, without any observable patterns. The location of the peak compressive stress was very similar for the tests, varying from 28μm to 47μm below the surface, except for the second test, which showed a non-decreasing trend throughout the profile. The only pattern recognizable for the machining parameters was that with increasing feed, peak compressive stress became less compressive, and the settling distance increased slightly.

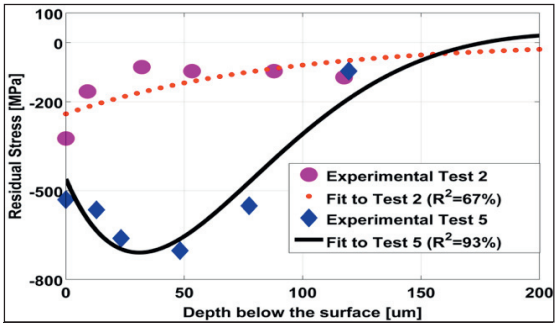

Figure 1: Worse (Test 2 at v_c=25 m/min and f=0.2 mm with R^2=67%) and best (Test 5 with R^2=93%) fit residual stress profiles

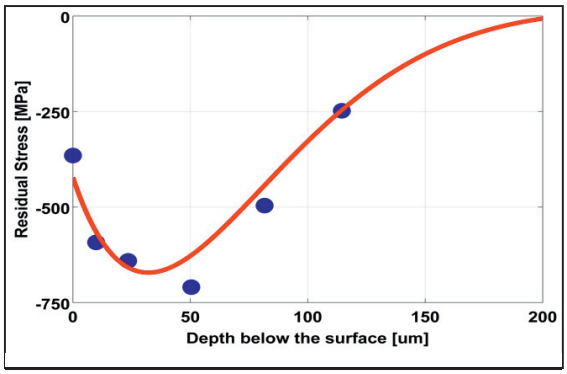

Figure 2: Validation of the model for GTD-111 at v_c=100 m/min and f=0.1 mm/rev

After finding the parameter effects, a middle point in feed with high cutting speed condition (last row in Table 1) was tested to validate the results (Figure 2). With sinusoidal decay function parameters predicted from obtained coefficients of other experiments, the predicted residual stress profile had R^2=91%, a significantly high prediction accuracy. This validation showed that it is possible to predict the residual stress profile within experimental ranges with good accuracy using a sinusoidal decay function fit.

Table 2 and Table 3 show the results of the model for face turned IN-100, in circumferential and radial directions respectively. Circumferential stresses showed R2 values greater than 95% for all tests, whereas radial stresses showed R2 values higher than 86%. Therefore, the model fit better to the experimental data for face turned IN-100 than end milled GTD-111. It is observed from the results that with increasing edge radius, surface residual stresses became more tensile in both circumferential and radial directions, and the settling distance increased for the radial residual stress. Also, with the addition of the TiAlN coating, peak compressive stresses became smaller (less compressive), and the settling and peak compressive stress locations got closer to the surface.

Table 1. Coefficients and results of the model for milling GTD-111

v_c	f	C	ς	ω_d	ϕ	R^2	PTS	PCS	PCD	SD
m/min	mm			m^{-1}	°	%	MPa	MPa	μm	μm
25	0.05	1444	0.71	16.6	101	91	-273	-570	36	184
25	0.2	241	0.98	2.3	178	67	-241	-241	0	244
50	0.05	5250	0.95	7.3	94	86	-388	-784	33	134
50	0.2	1604	0.72	9.2	109	79	-520	-705	47	313
100	0.05	1671	0.71	16.2	106	93	-470	-724	32	189
100	0.2	2294	0.94	9.6	95	75	-194	-382	28	115
100	0.1	1879	0.78	14	103	91	-423	-672	32	172

Table 2. Coefficients and results of the model for turning IN-100 (circumferential direction)

v_c	Edge	C	ς	ω_d	ϕ	R^2	PTS	PCS	PCD	SD
m/min				m^{-1}	°	%	MPa	MPa	μm	μm
24	Sharp	3420	0.89	11.5	82	95	478	-462	53	132
24	10μm	2539	0.71	12.8	71	97	807	-605	87	238
24	25μm	4792	0.94	6.5	80	98	851	-376	81	166
24	TiAlN	3349	0.92	60	-76	99	800	-20	55	58

Table 3. Coefficients and results of the model for turning IN-100 (radial direction)

v_c	Edge	C	ς	ω_d	ϕ	R^2	PTS	PCS	PCD	SD
m/min				m^{-1}	°	%	MPa	MPa	μm	μm
24	Sharp	4848	0.97	6.5	89	86	66	-439	41	120
24	10μm	1503	0.71	11.2	80	94	266	-413	87	274
24	25μm	7833	0.89	1.3	88	89	279	-1326	273	652
24	TiAlN	722	0.72	30.5	63	89	330	-148	42	100

5. Conclusions

This work targeted to propose a new method of modeling the residual stress profile after machining processes using a sinusoidal decay function, which may provide a better representation of the profile and hence lead to better predictions.

- Empirical model was built to fit a sinusoidal decay function to the residual stress measurements along the depth of the profile.
- Particle Swarm Optimization method was used to optimize the fit of the function by minimizing the error between the experimental data and the model profile. It was found that good model fit with mostly R^2=80-90% representation of the experimental data is possible using such a function.
- Using the optimized model, findings were confirmed by validating with an extra experiment, and a significantly good prediction was achieved (R^2=91%).

- Optimized model was used to obtain the four key residual stress measures that are the *PTS*, *PCS*, *PCD*, and *SD* for all the experiments. These can be directly determined for any set of experimental data from the fit function.
- Using these four key measures, effects of machining parameters such as the cutting speed, feed, cutting edge radius, and use of tool coating were investigated.
- It was found that the model fit the face turning experiments of IN-100 better than the end milling experiments of GTD-111.
- The findings of this study can be utilized to further improve the efforts of residual stress modeling with increased prediction accuracy.

Acknowledgements

The authors would like to acknowledge GE Power & Water for their support of this study. The authors also wish to thank the National Science Foundation for support of this work under Grant No. CMMI-1130780. Any opinions, findings, and conclusions or recommendations expressed in this material are those of the author(s) and do not necessarily reflect the views of the National Science Foundation.

References

[1] Ezugwu, E.O., Wang, Z.M., Machado, A.R., 1999. The Machinability of Nickel-Based Alloys: A Review, Journal of Materials Processing Technology 86, p. 1-61.
[2] Ulutan, D., Özel, T., 2011. Machining Induced Surface Integrity in Titanium and Nickel Alloys: A Review, International Journal of Machine Tools & Manufacture 51, p. 250-280.
[3] Jawahir, I.S., Brinksmeier, E., M'Saoubi, R., Aspinwall, D.K., Outeiro, J.C., Meyer, D., Umbrello, D., Jayal, A.D., 2011. Surface Integrity in Material Removal Processes: Recent Advances, CIRP Annals – Manufacturing Technology 60.2, p. 603-626.
[4] Ezugwu, E.O., Pashby, I.R., 1992. High Speed Milling of Nickel-Based Superalloys, Journal of Materials Processing Technology 33, p. 429-437.
[5] Darwish, S.M., 2000. The Impact of Tool Material and the Cutting Parameters on Surface Roughness of Supermet 718 Nickel Superalloy, Journal of Materials Processing Tech 97, p. 10-18.
[6] Arunachalam, R.M., Mannan, M.A., Spowage, A.C., 2004. Residual Stress and Surface Roughness When Facing Age Hardened Inconel 718 with CBN and Ceramic Cutting Tools, International Journal of Machine Tools and Manufacture 44, p. 879-887.
[7] Joshi, S.V., Vizhian, S.P., Sridhar, B.R., Jayaram, K., 2008. Parametric Study of Machining Effect on Residual Stress and Surface Roughness of Nickel Base Super Alloy UDIMET 720, Advanced Materials Research 47-50, p. 13-16.
[8] Ding, T.C., Zhang, S., Lv, H.G., Xu, X.L., 2011. A Comparative Investigation on Surface Roughness and Residual Stress during End-Milling AISI H13 Steel with Different Geometrical Inserts, Materials and Manufacturing Processes 26.8, p. 1085-1093.
[9] El-Axir, M.H., 2002. A Method of Modeling Residual Stress Distribution in Turning for Different Materials, International Journal of Machine Tools & Manufacture 42, p. 1055-1063.
[10] Brinksmeier, E., Cammett, J.T., König, W., Leskovar, P., Peters, J., Tönshoff, H.K., 1982. Residual Stresses – Measurement and Causes in Machining Processes, Annals of the CIRP 31.2, p. 491-510.
[11] Ulutan, D., Alaca, B.E., Lazoglu, I., 2007. Analytical Modelling of Residual Stresses in Machining, Journal of Materials Processing Technology183, p. 77-87.
[12] Fuh, K.H., Wu, C.F., 1995. A Residual-Stress Model for the Milling of Aluminum Alloy (2014-T6), Journal of Materials Processing Technology 51, p. 87-105.
[13] Yan, L., Yang, W., Jin, H., Wang, Z., 2012. Analytical Modeling of the Effect of the Tool Flank Wear Width on the Residual Stress Distribution, Machining Science and Technology: An International Journal 16.2, p. 265-286.
[14] Zhang, J.Y., Liang, S.Y., Zhang, G., Yen, D., 2006. Modeling of Residual Stress Profile in Finish Hard Turning, Materials and Manufacturing Processes 21.1, p. 39-45.
[15] Ji, X., Zhang, X., Liang, S.Y., 2013. Predictive Modeling of Residual Stress in Minimum Quantity Lubrication Machining, International Journal of Advanced Manufacturing Technology, DOI 10.1007/s00170-013-5439-2.
[16] Zhang, X., Ding, T.C., Li, J.F., 2012. Determination Surface and in-Depth Residual Stress Distributions Induced by Hard Milling of H13 Steel, Production Engineering Research Development 6. p. 375-383.
[17] Jacobus, K., DeVor, R.E., Kapoor, S.G., 2000. Machining-Induced Residual Stress: Experimentation and Modeling, Journal of Manufacturing Science and Engineering 122, p. 20-31.
[19] Lazoglu, I., Ulutan, D., Alaca, B.E., Engin, S., 2008. An Enhanced Analytical Model for Residual Stress Prediction in Machining, CIRP Annals – Manufacturing Technology 57, p. 81-84.
[20] Jiang, Y., Sehitoglu, H., 1994. An Analytical Approach to Elastic-Plastic Stress Analysis of Rolling Contact, Journal of Tribology 116, p. 577-587.
[21] Ee, K.C., Dillon Jr., O.W., Jawahir, I.S., 2005. Finite Element Modeling of Residual Stresses in Machining Induced by Cutting Using a Tool with Finite Edge Radius, International Journal of Mechanical Science 47, p.1611-1628.
[22] Outeiro, J.C., Ee, K.C., Dillon Jr., O.W., Wanigarathne, P.C., Jawahir, I.S., 2006. Some Observations on Comparing the Modeled and Measured Residual Stresses on the Machined Surface Induced by Orthogonal Cutting of AISI 316L Steel, *Proceedings of the 9th CIRP International Workshop on MMO*, Bled, Slovenia, March 17-19, 2006.
[23] Ulutan, D., Sima, M., Özel, T., 2011. Prediction of Machining Induced Surface Integrity Using Elastic-Viscoplastic Simulations and Temperature-Dependent Flow Softening Material Models in Titanium and Nickel-Based Alloys, Advanced Materials Research 223, p. 401-410.
[24] Özel, T., Ulutan, D., 2012. Prediction of Machining Induced Residual Stresses in Turning of Titanium and Nickel Based Alloys with Experiments and Finite Element Simulations, CIRP Annals – Manufacturing Technology 61, p. 547-550.
[25] Mittal, S., Liu. C.R., 1998. A Method of Modeling Residual Stresses in Superfinish Hard Turning, Wear 218, p. 21-33.
[26] Coello Coello, C.A., Pulido, G.T., Lechuga, M.S., 2004. Handing Multi-Objectives with Particle Swarm Optimization, IEEE Transactions on Evolutionary Computation 8.3, p. 256-279.
[27] Karpat, Y., Özel, T., 2007. Multi-Objective Optimization for Turning Processes Using Neural Network Modeling and Dynamic-Neighborhood Particle Swarm Optimization, International Journal of Advanced Manufacturing Technology 35, p. 234-247.
[28] Thepsonthi, T., Özel, T., 2012. Multi-Objective Process Optimization for Micro-End Milling of Ti-6Al-4V Titanium Alloy, International Journal of Advanced Manufacturing Technology 63, p. 903-914.
[29] Ulutan, D., Özel, T., 2013. Multiobjective Optimization of Experimental and Simulated Residual Stresses in Turning of Nickel-Alloy IN100, Materials and Manufacturing Processes 28, p. 835-841.